Three-Dimensional Metal-Organic Framework with Highly Polar Pore Surface: H-2 and CO2 Storage Characteristics

ARTICLE *in* INORGANIC CHEMISTRY · JUNE 2012

Impact Factor: 4.76 · DOI: 10.1021/ic202601y · Source: PubMed

5 AUTHORS, INCLUDING:

Sandeep Kumar Reddy
University of California, San Diego
12 PUBLICATIONS **161** CITATIONS
SEE PROFILE

Arpan Hazra
Jawaharlal Nehru Centre for Advanced Scienti…
12 PUBLICATIONS **174** CITATIONS
SEE PROFILE

Tapas Maji
Jawaharlal Nehru Centre for Advanced Scienti…
176 PUBLICATIONS **4,299** CITATIONS
SEE PROFILE

Inorganic Chemistry

Article

pubs.acs.org/IC

Three-Dimensional Metal–Organic Framework with Highly Polar Pore Surface: H_2 and CO_2 Storage Characteristics

Kolleboyina Jayaramulu,[†] Sandeep Kumar Reddy,[‡] Arpan Hazra,[†] Sundaram Balasubramanian,[‡] and Tapas Kumar Maji*,[†]

[†]Molecular Materials Laboratory and [‡]Molecular Modelling Laboratory, Chemistry and Physics of Materials Unit, Jawaharlal Nehru Centre for Advanced Scientific Research, Jakkur, Bangalore 560 064, India

Supporting Information

ABSTRACT: A three-dimensional (3D) pillared-layer metal–organic framework, $[Cd(bipy)_{0.5}(Himdc)](DMF)]_n$ (**1**), (bipy =4,4′-bipyridine and Himdc = 4,5-imidazoledicarboxylate) has been synthesized and structurally characterized. The highly rigid and stable framework contains a 3D channel structure with highly polar pore surfaces decorated with pendant oxygen atoms of the Himdc linkers. The desolvated framework $[Cd(bipy)_{0.5}(Himdc)]_n$ (**1′**) is found to exhibit permanent porosity with high H_2 and CO_2 storage capacities. Two H_2 molecules occluded per unit formula of **1′** and the corresponding heat of H_2 adsorption (ΔH_{H2}) is about ~9.0 kJ/mol. The high value of ΔH_{H2} stems from the preferential electrostatic interaction of H_2 with the pendent oxygen atoms of Himdc and aromatic bipy linkers as determined from first-principles density functional theory (DFT) based calculations. Similarly, DFT studies indicate CO_2 to preferentially interact electrostatically ($C^{\delta+}\cdots O^{\delta-}$) with the uncoordinated pendent oxygen of Himdc. It also interacts with bipy through C–H···O bonding, thus rationalizing the high heat (ΔH_{CO2} ~ 35.4 kJ/mol) of CO_2 uptake. Our work unveiled that better H_2 or CO_2 storage materials can be developed through the immobilization of reactive hetero atoms (O, N) at the pore surfaces in a metal–organic framework.

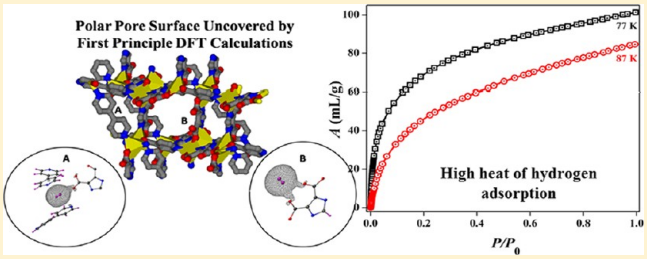

INTRODUCTION

Porous coordination polymers (PCPs) or metal–organic frameworks (MOFs) are widely regarded as promising functional materials for many applications such as gas storage,[1] catalysis,[2] separation,[3] luminescent sensing,[4] magnetic materials,[5] ion-exchange,[6] and even as delivery vehicles for controlled medicine.[7] In recent years, the synthesis and characterization of MOFs based on mixed ligand systems attracted considerable interest because of its control over (i) structural dimensionality, (ii) interpenetration, (iii) pore size, (iv) chemical environment and the polarity of the pore in the resulting MOF structure.[8] Many groups including ours have reported the porous properties particularly H_2 storage characteristics of the modified and tunable pore surfaces in MOF composed of mixed ligand systems.[8d−i] Recent research suggest that an energy of interaction of about 22–25 kJ/mol would be enough to maintain high capacity H_2 adsorption in porous materials at 298 K in the pressure range of 1.5–30 bar.[9] The immobilization of unsaturated metal sites in the coordination framework has been one of the successful methods for the increase of heat of H_2 adsorption,[10] and we have previously shown that an unsaturated alkali metal cation (K^I) has pronounced effect in the enhancement of heat of H_2 adsorption which was also supported by first principles calculations.[10a] MOFs with heterogeneous surface structure with local dipoles may enhance H_2 and CO_2 uptake capacity as they can interact more strongly than only through weak dispersion forces. Therefore, the inclusion of heteroatoms or highly electronegative atoms like F, O, or N in the pore surface is another effective way to increase adsorption energies for H_2 and CO_2.[11] Recently we and other groups showed that MOFs with fluorinated linkers have profound impact on the heat of H_2 adsorption, which has been correlated with the dipole induced dipole interactions.[11a−c] Similarly, the potential of fluorine or amine groups to interact with CO_2 is now reasonably well understood, as chemisorption by amines is an effective technology for removal of CO_2 from power plant flue gases. Recent results suggest that modifying the pore surface by incorporating Lewis basic sites (-amino, -pyrimidine, -hydroxo) or organic cations enhances low pressure CO_2 uptake and isosteric heat of adsorption.[11d−l] In this context 4,5-imidazoledicarboxylic acid (H_3imdc) is a versatile linker having three pH dependent abstractable protons and may provide diverse binding mode based on two imidazole nitrogen and four carboxylate oxygen atoms.[12] Therefore, a MOF composed of H_3imdc and aromatic linkers can afford several adsorption sites for electrostatic interactions with H_2 or CO_2 and can increase adsorption enthalpy. In this Article, we report the synthesis and structural characterization of a three-dimensional (3D) rigid metal–organic framework [Cd-

Received: December 2, 2011
Published: June 20, 2012

   dx.doi.org/10.1021/ic202601y | Inorg. Chem. 2012, 51, 7103–7111

$(bipy)_{0.5}(Himdc)](DMF)]_n$ (**1**), (bipy = 4,4′-bipyridine and H-imdc = 4,5-imidazoledicarboxylate) composed of mixed ligand system. It possesses high thermal stability and exhibits permanent porosity with moderate surface area. The framework shows 1.23 wt % uptake for H_2 at 77 K under high pressure with a high heat of adsorption (~9.0 kJ/mol). Similarly, the framework exhibits 23.5 wt % and 9.0 wt % CO_2 storage capacity at 195 and 298 K, respectively, with heat of adsorption of about 35.4 kJ/mol. The high heat adsorption can be attributed to the favorable interactions of H_2 or CO_2 with the pore surface. Using first principles calculations, we substantiate this energy quantitatively and unearth the nature of H_2/CO_2–MOF interactions from the detailed structures determined for various sites of interactions, and we demonstrate that hetero atoms (e.g., N, O) or aromatic sites on the pore surface are the favorable adsorption sites.

EXPERIMENTAL SECTION

Materials. All the reagents and solvents employed were commercially available and used as supplied without further purification. $Cd(NO_3)_2{\cdot}4H_2O$, 4,5-imidazoledicarboxylic acid, and 4,4′-bipyridine were obtained from Aldrich Chemical Co.

Physical Measurements. The elemental analyses were carried out using a Thermo Scientific Flash 2000 CHN analyzer. IR spectrum of the compound was recorded on a Bruker IFS 66v/S spectrophotometer using KBr pellet in the region 4000–400 cm^{-1}. Thermogravimetric analysis (TGA) was carried out on Mettler Toledo TGA850 instrument in the temperature range of 25–600 °C under nitrogen atmosphere (flow rate of 50 mL/min) at a heating rate of 3 °C/min. Powder X-ray diffraction (PXRD) studies in different state of the samples were recorded on a Bruker D8 Discover instrument using Cu–Kα radiation.

Synthesis of $[Cd(bipy)_{0.5}(Himdc)](DMF)]_n$ (1). $Cd(NO_3)_2{\cdot}4H_2O$ (0.25 mmol, 0.077 g) was dissolved in 12.5 mL of acetonitrile with constant stirring. 4,5-Imidazoledicarboxylic acid (H_3imdc) (0.25 mmol, 0.039 g) and 4,4′-bipyridine (bipy) (0.125 mmol, 0.0195 g) were dissolved in 12.5 mL of *N*,*N*-dimethylformamide (DMF) and stirred well for 30 min to make a homogeneous solution. Acetonitrile solution (2 mL) of $Cd(NO_3)_2$ was slowly and carefully layered on top of the ligand solution of DMF (2 mL) using the 2 mL buffer solution of acetonitrile and DMF (1:1). After two weeks colorless block type single crystals were grown at the junction of the two different solvents. The crystals were separated and washed with acetonitrile, which was subjected to X-ray diffraction. Yield: 80%. Anal. Calcd. for $C_{13}H_{13}N_4O_5Cd$: C, 37.44; H, 2.88; N, 13.44. Found: C, 37.35; H, 2.98; N, 13.24%. IR (KBr, cm^{-1}): ν(N–H), 3244; ν(C–H), 2928; ν_{as}(OCO), 1602; ν_s(OCO), 1368 and $\nu_s(Ar_{C=C})$1557.

Adsorption Measurements. Adsorption studies of N_2 (77 K), CO_2 (195 and 298 K) and H_2 (77 and 87 K) on the dehydrated samples prepared at 473 K under high vacuum, were carried out using a Quantachrome Autosorb-1C analyzer. The adsorption isotherm of different solvents (like CH_3CN, EtOH, and C_6H_6, at 298 K and MeOH at 293 K) were measured in the vapor state by using a BELSORP-aqua volumetric adsorption instrument from BEL, Japan. In the sample chamber (~12 mL) maintained at $T \pm 0.03$ K was placed the adsorbent sample (100–150 mg), which had been prepared at 473 K at 10^{-1} Pa for 18 h prior to measurement of the isotherms. The adsorbate was charged into the sample tube, and then the change of the pressure was monitored and the degree of adsorption was determined by the decrease of the pressure at the equilibrium state. All operations were computer-controlled and automatic. High-pressure H_2 (77 K) and CO_2, CH_4 (298 K) sorption measurements were carried out on a fully computer controlled volumetric BELSORP-HP, BEL Japan high pressure instrument. All the gases used for the high pressure measurements are scientific/research grade with 99.999% purity. For the measurements, an approximately 300 mg sample was taken in a stainless-steel sample holder and degassed at 493 K for a period of 18 h under 10^{-1} Pa vacuum. Dead volume of the sample cell was measured with helium gas of 99.999% purity. Nonideal correction for H_2 and CO_2 gases were made by applying virial coefficients at the respective measurement temperature.

X-ray Crystallography. A suitable single crystal of compound **1** was mounted on a thin glass fiber with commercially available super glue. X-ray single crystal structural data were collected on a Bruker Smart–CCD diffractometer equipped with a normal focus, 2.4 kW sealed tube X-ray source with graphite monochromated Mo–K_α radiation (λ = 0.71073 Å) operating at 50 kV and 30 mA, with ω scan mode. The program SAINT[13] was used for integration of diffraction profiles, and absorption correction were made with SADABS program.[14] The structure was solved by direct methods using SIR-92[15] and followed by successive Fourier and difference Fourier Syntheses. All the non-hydrogen atoms were refined anisotropically. Potential solvent accessible area or void space was calculated using the PLATON[16] multipurpose crystallographic software. All calculations were carried out using SHELXL 97,[17]SHELXS 97,[18] PLATON 99,[16] and WinGX system, ver. 1.70.01.[19] All crystallographic and structure refinement data of **1** are summarized below. Selected bond distances and angles are given in Supporting Information, Table S1.

Crystal Data of **1**. Formula $C_{13}H_{13}CdN_4O_5$, M_r = 417.62, Monoclinic, Space group *C*2/*c* (no. 15), a = 22.382(3) Å, b = 10.7731(15) Å, c = 13.5325(18) Å, β = 100.108(6)°, V = 3212.4(8) Å^3, Z = 8, ρ_{calc} =1.694 g cm^{-3}, μ(Mo–K_α) = 1.388 mm^{-1}, F(000) = 1592, T = 293 K, λ (Mo–K_α) = 0.71073 Å, θ_{max} = 26.3°, GOF = 1.14. A total of 17917 reflections were collected, of which 3237 were unique (R_{int} = 0.056). R_1= 0.0444 for 2771 independent reflections with $I > 2\sigma(I)$, w_{R2} = 0.1345 for all data.

Computational Details. Bulk periodic density functional theory (DFT) calculations were carried out using the plane wave code CPMD.[20] The super cell consisted of one unit cell of the metal–organic framework (MOF) and/or gas molecules (H_2 or CO_2). Solvent molecules were not included in modeling of these systems. Valence electrons were represented using a plane wave basis set with an energy cutoff of 80 Ry. The interaction of valence electrons with the core electrons and the nuclei were represented by a norm-conserving pseudopotential of Troullier and Martins type.[21] The gradient-corrected Becke, Lee, Yang, and Parr (BLYP) functional was employed[22] to treat the exchange and correlation interactions. Initial calculations consisted of iterative optimization of the cell parameters and atomic positions until a minimum energy configuration was found. Further, to identify the preferred locations of H_2 or CO_2 molecules in the MOF, molecular dynamics (MD) simulations using the Car–Parrinello method (CPMD)[23] were carried out at a temperature of 50 K. These were performed by constraining the MOF and allowing the gas molecules (H_2 or CO_2) to explore various regions within the framework as a function of time. Temperature was maintained through a Nose–Hoover chain thermostat[24] using a coupling constant of 3250 cm^{-1}. In these runs, the H_2 atoms were replaced by deuterium atoms so as to enable the use of a larger time step of 5 a.u. The trajectory was generated for 3 ps, and an animation demonstrated that the gas molecules explored all the regions of the pore(s). Locations of the gas molecules possessing low energies were identified from this trajectory. Direct optimization of the geometry (i.e., of the MOF and of the gas molecule) was initiated from such favored locations. Optimization of geometry was pursued until the maximum force on any atom was less than 10^{-4} a.u. Gas molecules are known to interact with MOF through van der Waals (vdW) forces in addition to other interactions.[25] While many methods to treat vdW interactions within the DFT formalism exist, an easier route is to add it as an empirical potential. In the present study, we have employed the vdW parameters of Grimme as derived for the BLYP functional.[26] The binding energy of the gas molecule (H_2 or CO_2) with the MOF is calculated using the following formula,

$$\Delta E = E(\text{MOF} + \text{gas}) - E(\text{MOF}) - n \times E(\text{gas})$$

where E(MOF + gas), E(MOF), and E(gas) represent the energies calculated for MOF with H_2 or CO_2, MOF and isolated gas molecule. Here, E(gas) was calculated in the same simulation box as that of the

dx.doi.org/10.1021/ic202601y | *Inorg. Chem.* 2012, 51, 7103–7111

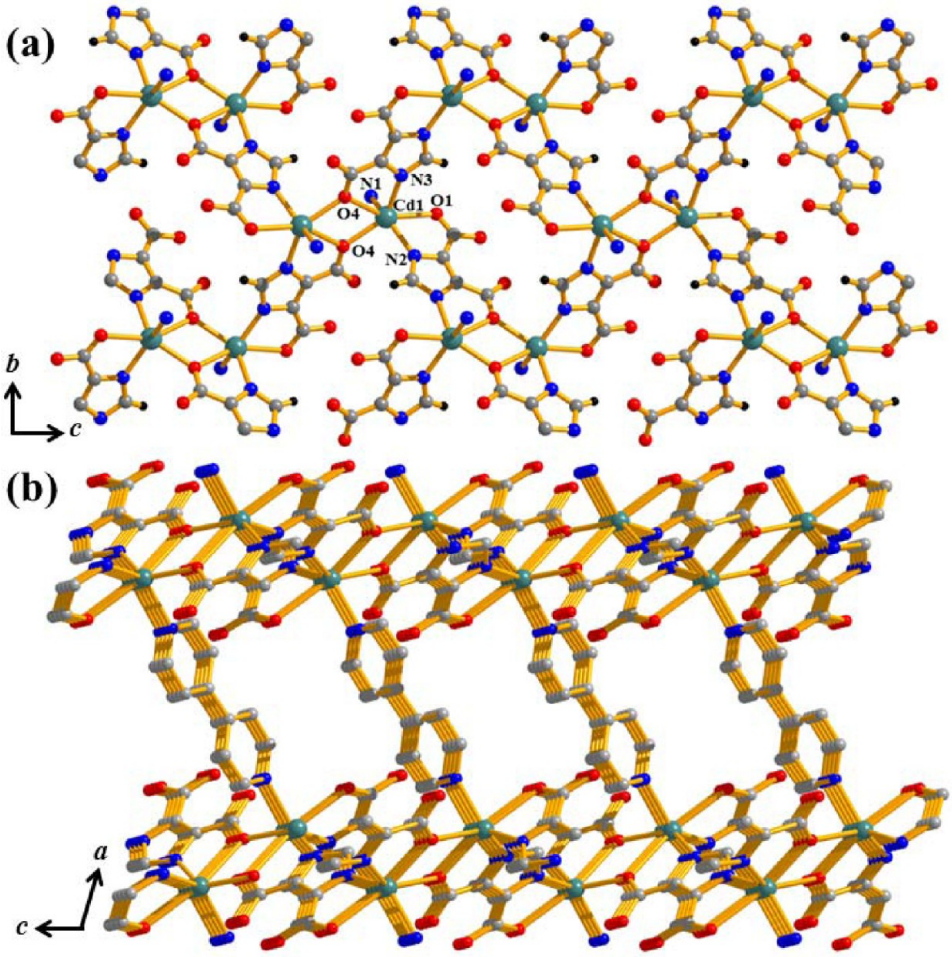

Figure 1. (a) View of the 2D corrugated sheet of $[Cd(Himdc)]_n$. (b) View of the 3D pillared-layer structure where parallel aligned bipy linkers connect the layers to form rectangular channels along the *b*-direction.

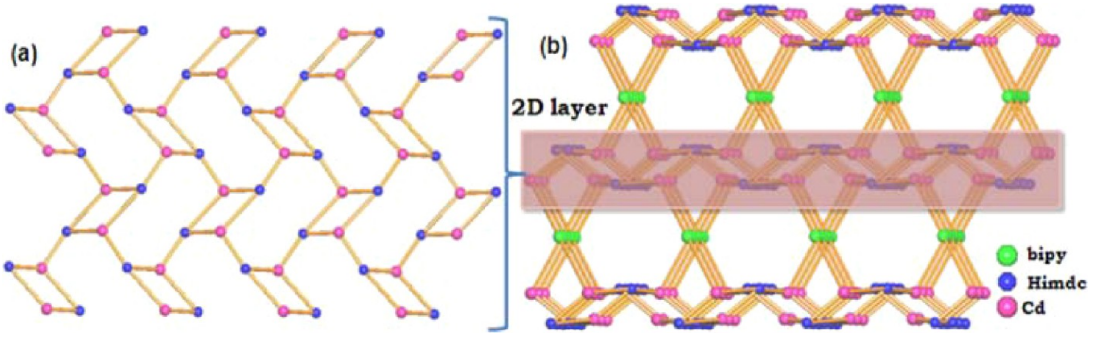

Figure 2. Network topology of compound **1** analyzed by TOPOS. (a) 3-connected uninodal 2D net; (b) 2,3,4-connected 3D framework formed by pillaring the 2D layer by bipy linker (simplifying Cd, Himdc, and bipy as a single node).

MOF and "*n*" gives the number of gas molecules present in the MOF. Thermal contributions to the binding energy were not considered. This contribution is expected to be less than 1 kJ/mol and would not change the results much. All the structures were visualized using Jmol[27] and VMD.[28]

RESULTS AND DISCUSSIONS

Structural Description of $[Cd(bipy)_{0.5}(Himdc)](DMF)]_n$ (1). Compound **1** crystallizes in the monoclinic *C*2/*c* space group (details in experimental part) and structure determination reveals a 3D pillared layer coordination framework of Cd(II) bridged by the Himdc and bipy linkers. The asymmetric unit of **1** consists of one octahedral Cd(II) atom, one Himdc, half bipy and one guest DMF molecule (Supporting Information, Figure S2a and Figure 1a). Each Himdc chelates to two Cd(II) centers through (N2, O1) and (N3, O4) atoms and connects to another Cd(II) through oxo(μ_2-O4) bridge and thus forming a two-dimensional (2D) $\{Cd(Himdc)_2\}$ corrugated layer in the crystallographic *bc* plane (Figure 1a). The dimeric fragments $Cd_2(\mu_2\text{-}O4)_2$ in the layer ($\angle$Cd−O4−Cd = 114.85(18)°, Cd···Cd = 4.047 Å) are connected in the axial coordination with bipy forming a 3D pillared-layer framework (Figure 1b). Structural analysis with TOPOS

dx.doi.org/10.1021/ic202601y | *Inorg. Chem.* 2012, 51, 7103−7111

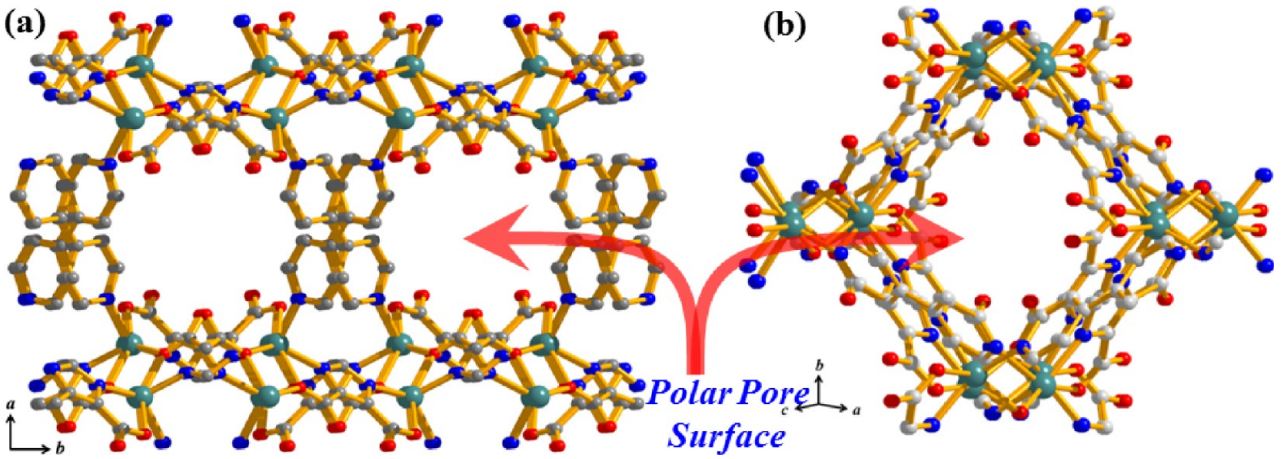

Figure 3. View of the 3D framework (a) along the *c*-axis showing oval shaped channels decorated with pendent carboxylate oxygen atoms and pyridyl moieties; (b) square shaped channels along perpendicular to *b*-axis decorated with pendent carboxylate oxygen atoms.

software[29] suggests the 2D layer is a 3-c uninodal net considering Cd1 and Himdc as a single node and the corresponding Schläfli symbol is $\{4.8^2\}$ (Figure 2a). The overall 3D framework reveals a 3-nodal 2,3,4-c net (Figure 2b) with stoichiometry (2-c)(3-c)2(4-c)2 and the corresponding Schläfli symbol for the net is $\{12\}\{4.8^2.12^3\}2\{4.8^2\}2$. In **1**, Cd1−O and Cd1−N bond distances are in the range of 2.319(4)−2.489(6) Å and 2.223(4)−2.271(5) Å, respectively (Supporting Information, Table S1). The degree of distortion from the ideal octahedral geometry is reflected in *cisoid* angles (range: 69.14(14)−134.13(15)°) and *transoid* angles (range: 137.94(18)−153.23(16)°) around Cd(II) (Supporting Information, Table S1). The bipy pillars are aligned parallel along the crystallographic *b*-axis and connecting diagonally the $\{Cd(Himdc)_2\}$ corrugated layers, to form rectangular channels with the dimensions of 3.84 × 1.06 $Å^2$ (Figure 1b and Supporting Information, Figure S2b). Moreover, along the *c*-axis bipy pillars are in a criss-cross and canted fashion supported by $\pi-\pi$ interactions which results in oval-shaped channels with dimension of 4.68 × 3.84 $Å^2$ (Figure 3a). It is worth mentioning that viewing along the perpendicular to *b*-axis framework also shows rectangular channels of dimension of 3.2 × 2.1 $Å^2$ (Figure 3b). The 3D channels are occupied by the guest DMF molecules, and each pore is decorated by the uncoordinated pendent oxygen atoms (O2, O3) from the Himdc and panels of bipy pillars, resulting in a highly polar pore surface (Supporting Information, Figure S2b and Figure 3b). The calculation using PLATON[16] suggest that the 3D framework contains 42.2% void space to the total crystal volume after removal of the guest DMF molecules. The Cd···Cd separation along the Himdc and bipy pillar is 8.894 and 11.596 Å, respectively.

Framework Stability. To study the framework stability of **1**, we performed thermogravimetric analysis (TGA) and powder X-ray diffraction (PXRD) studies after removal of the guest DMF molecules. TGA shows the loss of one DMF molecule in the temperature range of 30−200 °C (obs. wt. loss ~17.11% and calc. wt. loss ~17.45%) and the desolvated framework $[Cd(bipy)_{0.5}(Himdc)]_n$ (**1′**) is stable up to 250 °C (Supporting Information, Figure S3). Upon further heating, another weight loss was observed in the temperature range of 250−290 °C which corresponds to half of the bipy molecule (obs. wt. loss ~35.39% and calc. wt. loss ~36.45%) and later, the framework decomposes to unidentified product. The PXRD pattern of **1′** exhibits sharp lines without shifting the peak positions and intensities, suggesting that framework is highly rigid and robust (Supporting Information, Figure S4).

Permanent Porosity and Gas Storage Properties. Encouraged by the 3D channel structure, and the high thermal stability and structural rigidity, we determined the permanent porosity of the desolvated framework (**1′**). The N_2 (kinetic diameter = 3.6 Å)[30] adsorption isotherm shows typical type I profile, suggesting a microporous nature of the framework (Figure 4). The surface area calculated from the Langmuir

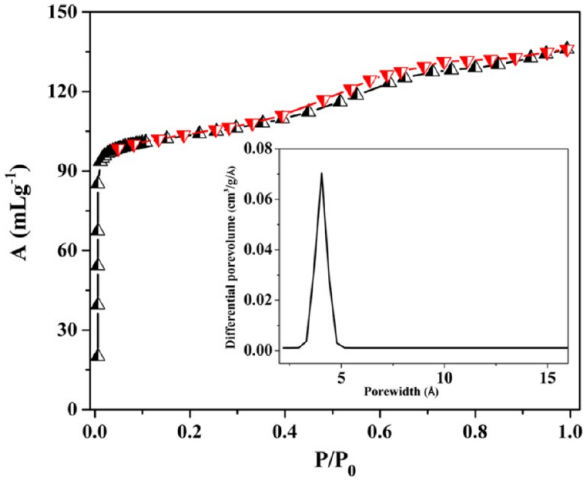

Figure 4. N_2 sorption isotherm for **1′** at 77 K. (Inverted red triangles are for adsorption and black triangles are for desorption). Inset: Pore volume versus pore size distribution by the S−F method.

equation is about 648.8 m^2/g, and the corresponding Brunauer−Emmett−Teller (BET) surface area is 498.12 m^2/g. The slight discrepancy between the measured pore volume (0.22 cm^3/g) from the N_2 adsorption isotherm and the value calculated from the single-crystal X-ray structure (0.29 cm^3/g) using PLATON is possibly due to the inability of N_2 molecules to effectively enter into the small pores at 77 K. This happens owing to some energy barrier or blocking of pores by strongly adsorbed N_2 molecules. The inset to Figure 4 shows the differential pore volume distributions as functions of pore width calculated by the Saito−Foley (S−F)[31] method which suggests that the pore size is about 4.6 Å. This agrees well with the pore

dx.doi.org/10.1021/ic202601y | *Inorg. Chem.* 2012, 51, 7103−7111

size obtained from single crystal structure. We have measured H_2 storage capacity of **1′** at 77 and 87 K up to 1 atm (P/P_0 = 1), and the profile shows steep uptake at low pressure region which was ended without saturation (inset to Figure 5). The final

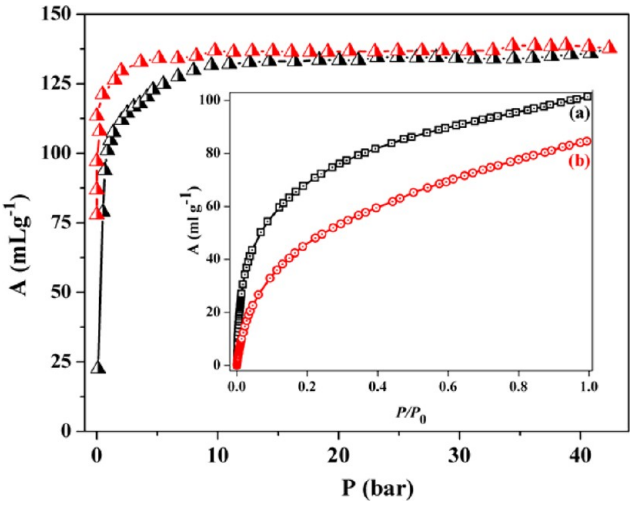

Figure 5. High-pressure H_2 sorption isotherms for **1′** at 77 K; inset: H_2 sorption profile at 77 K (a) and 87 K (b) up to 1 atm.

uptake amounts are 101 and 84 mL/g which match up about of 0.9 and 0.75 wt % storage capacity. Excess high pressure H_2 adsorption capacity of **1′** was measured with the BELSORP HP apparatus at 77 K, and the corresponding storage capacity was found to be 1.23 wt % (Figure 5). The steep uptake at low pressure regions (up to 3 bar) suggests strong interaction of H_2 with the pore surface of **1′** decorated with the pendent oxygen atoms (O2 and O3) from the Himdc linker and aromatic π-cloud. The framework saturated with respect to H_2 at 77 K at about 10 bar and the saturated amount indicates about two H_2 molecules inclusion per formula unit of **1′**. The heat of H_2 adsorption (ΔH_{ads}) was derived from the Clausius−Clapeyron equation,[32a,11b] and the value is ΔH_{ads} = 13.3 kJ/mol at the low coverage regions (see details in Supporting Information, Figures S5−S7). This value is compatible with the highest reported value of ΔH_{ads} in MOF systems.[32b] However, the value calculated using the Clausius−Clapeyron approach exhibits a sudden rising behavior at low coverage. We have thus used an alternate virial[38] method which reduces to Henry's law from which the isosteric heat of adsorption is calculated to be 9.0 kJ/mol (see Supporting Information, Figures S8, S9).

The CO_2 gas sorption isotherms of **1′** measured at 195 and 298 K are shown in Figure 6. The adsorption isotherm at 195 K shows a two steps process with a small hysteresis (Figure 6a). The two step adsorption process is clearly evident from the plot of log(P/P_0) vs uptake (inset Figure 6). In the initial step, it uptakes 64 mL/g (12.15 wt % at STP) in the range of P/P_0 ∼ 0.001−0.055. In the next step, the framework adsorbs about 36 mL (7.07 wt %) up to P/P_0 ∼1. Such stepwise, hysteretic pressure dependent adsorption of CO_2 uptake has been observed in several flexible and dynamic porous MOFs, which respond to specific adsorbate molecules by means of a breathing or gate opening process related to structural expansion or close-open pore system.[8f,33] However, stepwise adsorption in a rigid framework is extremely rare and could stem from different adsorption sites. The small hysteresis and steep uptake at the low pressure region is indicative of strong

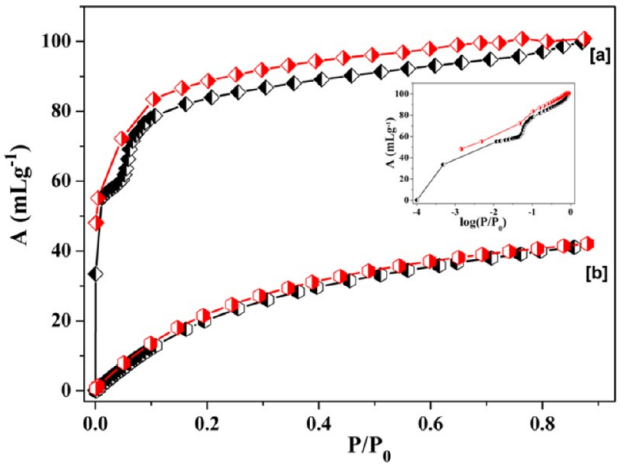

Figure 6. CO_2 sorption profile for **1′** at (a) 195 K and (b) 298 K. Inset: log profile showing the double step adsorption.

interaction of the CO_2 molecules with the pore surface. The isosteric heat of adsorption ($q_{st,\phi}$), calculated using the Dubinin−Radushkevich (DR) equation,[34] is about 35.4 kJ/mol. The CO_2 storage capacity at 298 K up to 1 atm is ∼9 wt % (Figure 6b) which significantly increases to ∼11.4 wt % at high pressure (Figure 7a). It is worth mentioning that the saturation

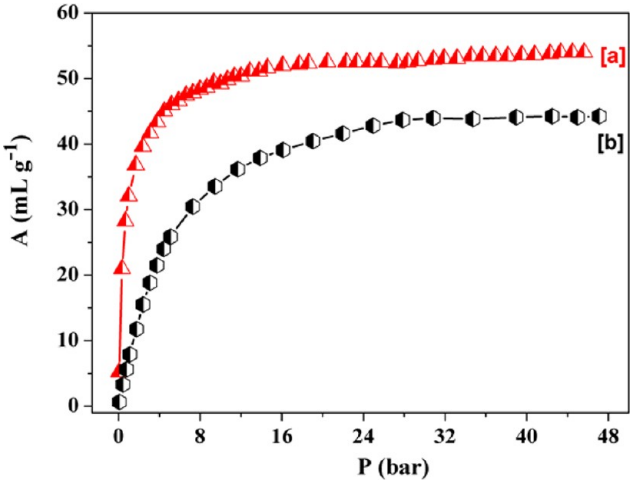

Figure 7. (a) CO_2 and (b) CH_4 sorption profile for **1′** measured at 298 K.

amount at high pressure measurement shows commensurate adsorption with about one molecule of CO_2 inclusion per formula unit of **1′**, and no double-step profile was observed. Moreover, the corresponding methane storage capacity of **1′** suggests about 6.5 wt % at 298 K up to 48 bar (Figure 7b). The pore surfaces are decorated with the pendent oxygen atoms (O2 and O4) from the Himdc linker, and the π-cloud of pyridyl ring of bipy, which gives rise to an electric field in the host framework, can interact with the quadrupole moment of CO_2 (-1.4×10^{-39} C m^2) providing additional energy for adsorption.

Solvent Adsorption Study. Inspired by the highly active pore surface in **1′**, we anticipated interesting sorption behavior with solvent molecules depending upon the polarity (Lewis basicity) of guest molecules. To analyze the effect of small molecules on the pore surfaces, we have carried out a vapor

dx.doi.org/10.1021/ic202601y | Inorg. Chem. 2012, 51, 7103−7111

sorption study with different solvent molecules (methanol (MeOH), ethanol (EtOH), acetonitrile (CH_3CN), and benzene (C_6H_6)) of varying size and polarity. The sorption profiles of MeOH (3.8 Å), CH_3CN (4.0 Å), and EtOH (4.3 Å) reveal a type I curve with small hysteresis and sorption amount increases with increasing pressure (Figure 8). Moreover,

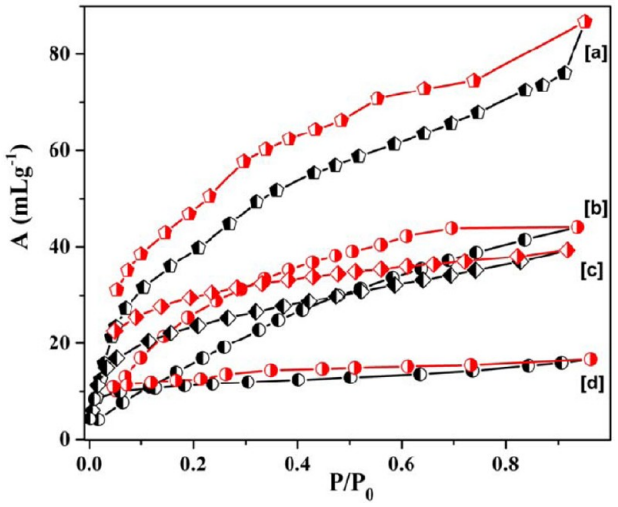

Figure 8. Vapor sorption isotherm for **1′**. (a) MeOH (293 K); (b) EtOH (298 K); (c) CH_3CN (298 K); and (d) C_6H_6 (298 K).P_0 is the saturated vapor pressure of the adsorbates at the respective temperatures.

consistent with the smaller pore size and polarity of **1′**, no significant uptake of C_6H_6 (5.8 Å) is observed (Figure 8d). The calculations using the final sorption amount of MeOH, EtOH and CH_3CN suggest an uptake of 1.3, 0.72, and 0.58 molecules, respectively per formula unit of **1′**. All the profiles were analyzed by the DR equation and the values of βE_0, which reflect adsorbate−adsorbent affinity, are 7.59 kJ/mol for MeOH, 4.36 kJ/mol for EtOH, and 3.56 kJ/mol for CH_3CN. This also reflects the high polarity of the pore surfaces as among all the guest solvent molecules MeOH is the most polar and can interact effectively through different hydrogen-bonding (O−H···O/N) interactions between pendant and coordinated oxygen and nitrogen atoms from Himdc or bipy linker compared to EtOH and CH_3CN molecules.

Theoretical Study. To better understand the ability of the framework to store H_2 and CO_2 and the origin of high heat of H_2 and CO_2 adsorption in different experiments, we have carried out DFT calculations augmented by empirical van der Waals correction terms as described in detail in the experimental part later. Favorable adsorption sites for H_2 and CO_2 within the MOF and their energies have been determined. Many people have explained successfully the adsorption of gas molecules in MOFs using computational methods.[35] In the current work, geometry optimization runs were initiated from many configurations in each of which the gas molecule was positioned in a different location inside the MOF pore. In addition, CPMD simulations at 50 K were also carried out, to identify low energy positions for the H_2 and CO_2 molecules. The optimal positions of the H_2 and CO_2 molecule in the MOF channel are shown in Figure 9. For H_2, the experimental heat of adsorption (varying between 9.0 and 13.3 kJ/mol depending upon the method used) is reproduced when two H_2 molecules interact with the MOF and the calculated value is −12.88 kJ/

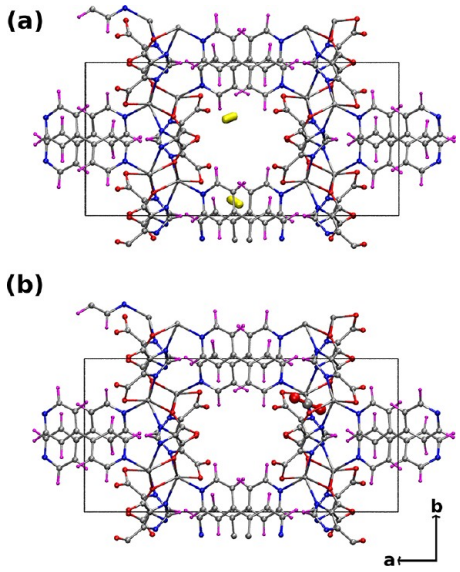

Figure 9. Locations of the (a) two H_2 molecules (shown as yellow tube) (top panel) and (b) one CO_2 molecule (bottom panel) as determined using DFT calculations. The molecules are present in the oval shaped channels of the crystal viewed along the *c*-axis.

mol. Figure 10a shows the positions of the two molecules, named as H_2−I and H_2−II, yielding this value. The contribution of the individual H_2 molecule to the total adsorption energy was also calculated, and the values are −5.74 and −8.00 kJ/mol for H_2−I and H_2−II molecules, respectively. The sum of these two values is not equal to the calculated total heat of adsorption mentioned earlier (−12.88 kJ/mol) because of minor variations in the optimized MOF coordinates between each of these three runs. Table 1 shows the binding energies of H_2 and CO_2 molecules with the MOF. van der Waals (vdW) corrections to the DFT energies are seen to be crucial to obtain a good comparison to experimental heats of adsorption, for both the gases. To identify the atoms of MOF interacting with adsorbate and thus to understand the nature of interactions, we have studied differences of electron densities. Figure 10b and 10c show the difference plot of electron density. It is calculated as $\rho(\text{MOF} + H_2) - \rho(\text{MOF}) - \rho(H_2)$, where ρ is the electron density and the latter two terms are calculated for the pure MOF and for a H_2 molecule in the gas phase, respectively. A change in electron density of MOF atoms surrounding the H_2 molecules can be clearly seen. H_2−I molecule lies nearly in the plane of the imidazolium ring with one of its atoms slightly positively charged. The latter interacts electrostatically with the two free oxygens (O2 and O3) of the carboxylate groups of the Himdc linker (Figure 10a). The distances of this H_2 atom from these two free oxygen atoms are 2.62 and 2.69 Å. The H_2−II molecule interacts in two ways: one is the electrostatic interaction between H_2 and the oxygen (O1) (which is bonded to metal atom) atoms, and other is the interaction of the π-electron cloud over the pyridine ring with the H_2 molecule. This H_2 molecule is at a distance of 2.61 Å from the oxygen atom (O1), and it lies between two pyridine rings at almost equal distance from both, with its molecular axis parallel to the plane of each ring (Figure 10a). The distances of this H_2 atom from these two free oxygen atoms are 2.62 and 2.69 Å. The binding energy for CO_2 adsorption is calculated to be −39.14 kJ/mol which is slightly higher than the experimental estimate of −35.4 kJ/mol. This overestimate

dx.doi.org/10.1021/ic202601y | *Inorg. Chem.* 2012, 51, 7103−7111

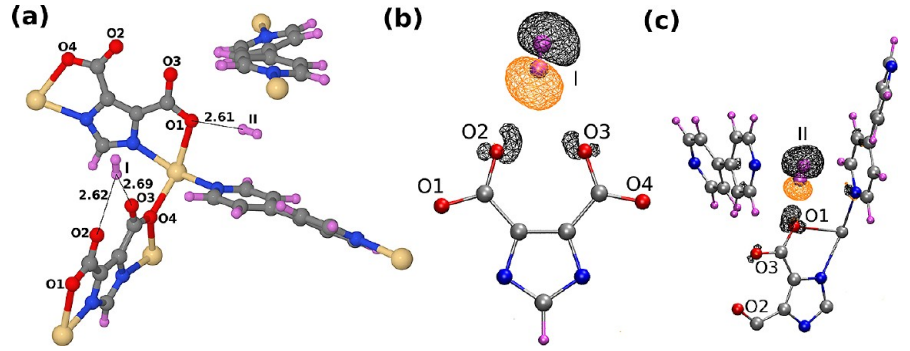

Figure 10. (a) Environment around the two adsorbed H_2 molecules at two different sites I and II as obtained from DFT calculations (distances are in Å). (b, c) Isosurface of the difference in the electron density of the system due to the adsorption of the H_2 molecules at I and II sites, respectively. Negative and positive values of electron density difference are shown in orange and black, respectively. Isosurface value is 0.0003 a.u. [Color code: C, gray; H, magenta; N, blue; O, red. Other atoms of MOF are not shown for clarity].

Table 1. Binding Energies of H_2 and CO_2 Molecules in the MOF Calculated Using BLYP/85 Ry Level of Theory with[26] and without Empirical van der Waals Corrections Compared against Experimental Values of the Heat of Adsorption[a]

	H_2	CO_2
BLYP	−6.14	−6.44
BLYP + vdW	−12.88	−39.14
Experiment	−9.0[b] (−13.3)[c]	−35.4[d]

[a]The energies are in kJ/mol. [b]Adsorption enthalpy value based on virial method. [c]Based on Clausius−Clapeyron equation. [d]Adsorption enthalpy value based on Dubinin− Radushkevich (DR) equation.

could be possibly due to the vdW parameters employed here. These were originally developed to describe systems in the gas phase. It has been recently shown that these parameters could overestimate the vdW contribution to the total energy in the condensed state.[36] One needs a good qualitative description of these long-range interactions in periodic systems to be able to accurately reproduce the experimental heats of adsorption. The environment around the CO_2 molecule present within the MOF is shown in Figure 11a. We identify three possible kinds of interaction between CO_2 and MOF, based purely on its location. The primary contribution to the binding energy is likely to come from the interaction of the electron deficient carbon atom of CO_2 with the lone pairs of the two free oxygen atoms (O2 and O3) of carboxylate groups as shown in Figure 11a. This molecule is at a distance of 2.95 and 3.21 Å from the two oxygens with its molecular axis parallel to the plane of imidazolium ring. A slight deviation of the backbone angle of CO_2 to a value of 178.1° is seen, with the carbon of the CO_2 bending toward the two free oxygen atoms.[37] The observed asymmetry in the measured distances from the carbon atom to the two carboxylate (free) oxygens is due to the existence of very weak hydrogen-bonding between one of the oxygen atoms of the CO_2 molecule and the acidic hydrogen of imidazolium ring as shown in Figure 11a. The hydrogen bond distance is 2.79 Å and angle is 105.8°. This system is possibly further stabilized by a Coulombic interaction between the two oxygen atoms of CO_2 and the hydrogens of the pyridine ring. All these interactions are clearly captured in a plot of the difference in the electron density brought upon the system because of the adsorption of CO_2, shown in Figure 11b.

CONCLUSIONS

In summary, a pillared-layer framework of Cd(II), $[Cd(bipy)_{0.5}(Himdc)](DMF)]_n$ (**1**), (bipy = 4,4′-bipyridine and Himdc = 4,5-imidazoledicarboxylate) with 3D channel structure composed of mixed ligand system has been successfully synthesized and characterized. The desolvated framework **1′** shows permanent porosity and high H_2 and CO_2 uptake characteristics. The high adsorption energy for H_2 (estimated to be between 9.0 and 13.3 kJ/mol depending

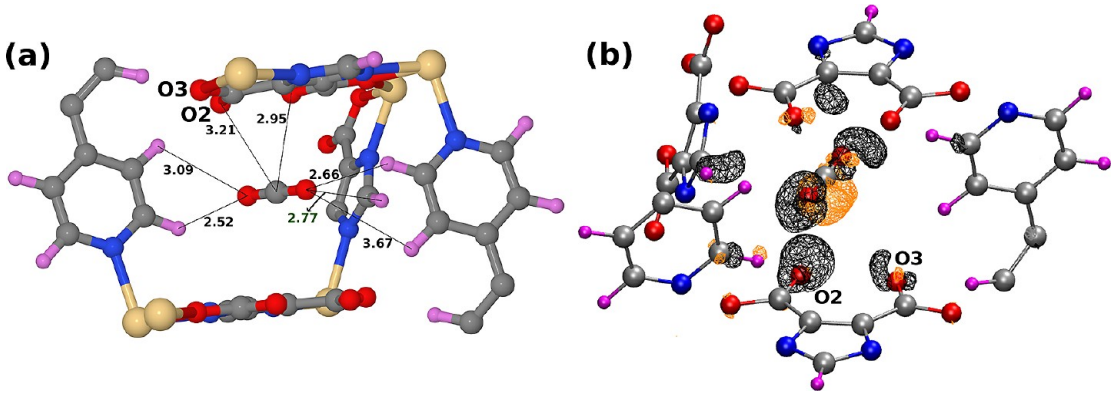

Figure 11. (a) View of the environment around the adsorbed CO_2 molecule obtained from DFT calculations (measured distances are in Å). Other atoms of the MOF are not shown for the sake of clarity. (b) Isosurface of the difference in the electron density of the system due to the adsorption of CO_2 molecule. Negative and positive electron density differences are shown in orange and black respectively. The isosurface value is 0.0006 a.u. [Color code: C, gray; H, magenta; N, blue; O, red. Other atoms of MOF are not shown for clarity].

dx.doi.org/10.1021/ic202601y | Inorg. Chem. 2012, 51, 7103−7111

upon the method used) and CO_2 (~35.4 kJ/mol) in **1′** is realized by the interactions with pendant oxygen atoms and aromatic pyridyl moieties. DFT calculations quantitatively agree with the experimental values of heat of adsorption and are also able to uncover the nature of interactions between H_2 (or CO_2) with the atoms of the MOF. This has been made possible through detailed structure analyses augmented by an analysis of the electron density. The experimental and theoretical investigations unequivocally suggest that the high polarity of the pore surfaces decorated by the oxygen atoms and aromatic rings provide significant contribution for the high heat of adsorption values. Thus, by modulating the pore environment via immobilizing the hetero atoms (N, O, F) in the pore surface, the gas adsorption properties of the resulting MOF can be fine-tuned. This affords a methodology for the development of high capacity of H_2/CO_2 storage materials that may operate at ambient conditions which is significant in the context of global energy and environment issues.

■ ASSOCIATED CONTENT

Ⓢ Supporting Information

Crystallographic data in CIF format. Further details are given in Figures S1−S4. This material is available free of charge via the Internet at http://pubs.acs.org.

■ AUTHOR INFORMATION

Corresponding Author

*E-mail: tmaji@jncasr.ac.in. Phone: +91 80 2208 2826. Fax: +91 80 22082766.

Notes

The authors declare no competing financial interest.

■ ACKNOWLEDGMENTS

S.B. acknowledges the Centre for Development of Advanced Computing, Bangalore for providing computational resources. The financial support (TKM) from Department of Science and Technology (Govt. of India) is gratefully acknowledged. K.J.R. and S.K.R is grateful to the UGC and CSIR, SRF India, for senior research fellowships.

■ REFERENCES

(1) (a) Li, H.; Eddaoudi, M.; O'Keeffe, M.; Yaghi, O. M. *Nature* **1999**, *402*, 276. (b) Maji, T. K.; Kitagawa, S. *Pure. Appl. Chem.* **2007**, *79*, 2155. (c) Eddaoudi, M.; Kim, J.; Rosi, N.; Vodak, D.; Wachter, J.; O'Keeffe, M.; Yaghi, O. M. *Science* **2002**, *295*, 469. (d) Vaidhyanathan, R.; Iremonger, S. S.; Dawson, K. W.; Shimizu, G. K. H. *Chem. Commun.* **2009**, *35*, 5230. (e) Thallapally, P. K.; Tian, J.; Motkuri, R. K.; Fernandez, C. A.; Dalgarno, S. J.; McGrail, B. P.; Warren, J. E.; Atwood, J. L. *J. Am. Chem. Soc.* **2008**, *130*, 16842.

(2) (a) Farrusseng, D.; Aguado., S.; Pinel, C. *Angew. Chem., Int. Ed.* **2009**, *48*, 7502. (b) Ma, L. Q.; Abney, C.; Lin, W. B. *Chem. Soc. Rev.* **2009**, *38*, 1248. (c) Ohmori, O.; Fujita, M. *Chem.Commun.* **2004**, 1586.

(3) (a) Gedrich, K.; Senkovska, I.; Klein, N.; Stoeck, U.; Henschel, A.; Lohe, M. R.; Baburin, I. A.; Mueller, U.; Kaskel, S. *Angew. Chem., Int. Ed.* **2010**, *49*, 8489. (b) Gu, Z. Y.; Yan, X. P. *Angew. Chem., Int. Ed.* **2010**, *49*, 1477. (c) Li, J. R.; Kuppler, R. J.; Zhou, H. C. *Chem. Soc. Rev.* **2009**, *38*, 1477. (d) Horike, S.; Shimomura, S.; Kitagawa, S. *Nat. Chem.* **2009**, *1*, 695.

(4) (a) Takashima, Y.; Martinez, V. M.; Furukawa, S.; Kondo, M.; Shimomura, S.; Uehara, H.; Nakahama, M.; Sugimoto, K.; Kitagawa, S. *Nat. Commun.* **2011**, *2*, 168. (b) Jayaramulu, K.; Kanoo, P.; George, S. J.; Maji, T. K. *Chem. Commun.* **2010**, *46*, 7906. (c) Allendorf, M. D.; Bauer, C. A.; Bhakta, R. K.; Houk, R. J. T. *Chem. Soc. Rev.* **2009**, *38*, 1330. (d) Rocha, J.; Carlos, L. D.; Paz, F. A. A.; Ananias, D. *Chem. Soc. Rev.* **2011**, *40*, 926.

(5) (a) Kurmoo, M. *Chem. Soc. Rev.* **2009**, *38*, 1353. (b) Nagaraja, C. M.; Behera, J. N.; Maji, T. K.; Pati, S. K.; Rao, C. N. R. *Dalton Trans.* **2010**, *39*, 6947. (c) Du, M.; Bu, X. H. *Prog. Chem.* **2009**, *21*, 2458. (d) Jia, H. P.; Li, W.; Ju, Z. F.; Zhang, J. *Eur. J. Org. Chem.* **2006**, *4*, 4264.

(6) (a) Maji, T. K.; Matsuda, R.; Kitagawa, S. *Nat. Mater.* **2007**, *6*, 142. (b) Tzeng, B. C.; Chiu, T. H.; Chen, B. S.; Lee, G. H. *Chem.—Eur. J.* **2008**, *14*, 5237. (c) Muthu, S.; Yip, J. H. K.; Vittal, J. J. *Chem. Soc., Dalton Trans.* **2002**, 4561. (d) Procopio, E. Q.; Linares, F.; Montoro, C.; Colombo, V.; Maspero, A.; Barea, E.; Navarro, J. A. R. *Angew. Chem., Int. Ed.* **2010**, *49*, 7308. (e) Suh, M. P.; Cheon, Y. E.; Lee, E. Y. *Coord. Chem. Rev.* **2008**, *252*, 1007. (f) Zhang, J. J.; Zhao, Y.; Gamboa, S. A.; Munoz, M.; Lachgar, A. *Eur. J. Inorg. Chem.* **2008**, *19*, 2982.

(7) (a) Horcajada, P.; Serre, C.; Maurin, G.; Ramsahye, N. A.; Balas, F.; Vallet-Regi, M.; Sebban, M.; Taulelle, F.; Ferey, G. *J. Am. Chem. Soc.* **2008**, *130*, 6774. (b) Hinks, N. J.; McKinlay, A. C.; Xiao, B.; Wheatley, P. S.; Morris, R. E. *Microporous Mesoporous Mater.* **2010**, *129*, 330. (c) Horcajada, P.; Serre, C.; Vallet-Regi, M.; Sebban, M.; Taulelle, F.; Ferey, G. *Angew. Chem., Int. Ed.* **2006**, *45*, 5974. (d) Imaz, I.; Rubio-Martínez, M.; García Fernández, L.; García, F.; Ruiz-Molina, D.; Hernando, J.; Puntes, V.; Maspoch, D. *Chem. Commun.* **2010**, *46*, 4737. (e) Lin, W. B.; Rieter, W. J.; Taylor, K. M. L. *Angew. Chem., Int. Ed.* **2009**, *48*, 650. (f) Taylor-Pashow, K. M. L.; Della Rocca, J.; Huxford, R. C.; Lin, W. B. *Chem. Commun.* **2010**, *46*, 5832.

(8) (a) Higuchi, M.; Tanaka, D.; Horike, S.; Sakamoto, H.; Nakamura, K.; Takashima, Y.; Hijikata, Y.; Yanai, N.; Kim, J.; Kato, K.; Kubota, Y.; Takata, M.; Kitagawa, S. *J. Am. Chem. Soc.* **2009**, *131*, 10336. (b) Tanaka, D.; Nakagawa, K.; Higuchi, M.; Horike, S.; Kubota, Y.; Kobayashi, T. C.; Takata, M.; Kitagawa, S. *Angew. Chem., Int. Ed.* **2008**, *47*, 3914. (c) Fukushima, T.; Horike, S.; Inubushi, Y.; Nakagawa, K.; Kubota, Y.; Takata, M.; Kitagawa, S. *Angew. Chem., Int. Ed.* **2010**, *49*, 4820. (d) Burrows, A. D. *CrystEngComm* **2011**, *13*, 3623. (e) Ma, B. Q.; Mulfort, K. L.; Hupp, J. T. *Inorg. Chem.* **2005**, *44*, 4912. (f) Kanoo, P.; Sambhu, R.; Maji, T. K. *Inorg. Chem.* **2011**, *50*, 400. (g) Park, H. J.; Suh, M. P. *Chem.—Eur. J.* **2008**, *14*, 8812. (h) Kanoo, P.; Maji, T. K. *Eur. J. Inorg. Chem.* **2010**, 3762. (i) Kanoo, P.; Matsuda, R.; Higuchi, M.; Kitagawa, S.; Maji, T. K. *Chem. Mater.* **2009**, *21*, 5860.

(9) Garrone, E.; Bonelli, B.; Otero Area, C. *Chem. Phys. Lett.* **2008**, *456*, 68.

(10) (a) Mohapatra, S.; Hembram, K.; Waghmare, U.; Maji, T. K. *Chem. Mater.* **2009**, *21*, 5406. (b) Rowsell, J. L. C.; Yaghi, O. M. *Angew. Chem., Int. Ed.* **2005**, *44*, 4670. (c) Dailly, M. D. A.; Liu, Y.; Brown, C. M.; Neumann, D. A.; Long, J. R. *J. Am. Chem. Soc.* **2006**, *128*, 16876. (d) Kaye, S. S.; Long, J. R. *J. Am. Chem. Soc.* **2008**, *130*, 806.

(11) (a) Hulvey, Z.; Sava, D. A.; Eckert, J.; Cheetham, A. K. *Inorg. Chem.* **2011**, *50*, 403. (b) Hazra, A.; Kanoo, P.; Maji, T. K. *Chem. Commun.* **2011**, *47*, 538. (c) Uemura, K.; Maeda, A.; Maji, T. K.; Kanoo, P.; Kita, H. *Eur. J. Inorg. Chem.* **2009**, 2329. (d) Feréy, G.; Latroche, M.; Serre, C.; Millange, F.; Loiseau, T.; Gan, A. P. G. *Chem. Commun.* **2003**, 2976. (e) Rowsell, J. L. C.; Yaghi, O. M. *J. Am. Chem. Soc.* **2006**, *128*, 1304. (f) Dincã, M.; Dailly, A.; Tsay, C.; Long, J. R. *Inorg. Chem.* **2008**, *47*, 11. (g) Vaidhyanathan, R.; Iremonger, S. S.; Shimizu, G. K. H.; Boyd, P. G.; Alavi, S.; Woo, T. K. *Science* **2010**, *330*, 650. (h) Demessence, A.; D'Alessandro, D. M.; Foo, M. L.; Long, J. R. *J. Am. Chem. Soc.* **2009**, *131*, 8784. (i) Kanoo, P.; Ghosh, A. C.; Cyriac, S.; Maji, T. K. *Chem.—Eur. J.* DOI: 10.1002/Chem.20110118. (j) Chen, S. M.; Zhang, J.; Wu, T.; Feng, P. Y.; Bu, X. H. *J. Am. Chem. Soc.* **2009**, *131*, 16027. (k) Caskey, S. R.; Wong-Foy, A. G.; Matzger, A. J. *J. Am. Chem. Soc.* **2008**, *130*, 10870. (l) An, J.; Rosi, N. L. *J. Am. Chem. Soc.* **2010**, *132*, 5578.

(12) (a) Gurunatha, K. L.; Uemura, K.; Maji, T. K. *Inorg. Chem.* **2008**, *47*, 6578. (b) Maji, T. K.; Mostafa, G.; Chang, H. C.; Kitagawa, S. *Chem. Commun.* **2005**, 2436. (c) Gu, J.-Z.; Lu, W.-G.; Jiang, L.; Zhou, H. C.; Lu, T.-B. *Inorg. Chem.* **2007**, *46*, 5837. (d) Lu, W. G.; Su, C. Y.; Lu, T. B.; Jiang, L.; Chen, J. M. *J. Am. Chem. Soc.* **2006**, *128*, 34.

(e) Liu, Y. L.; Kravtsov, V.; Larsen, R.; Eddaoudi, M. *Chem. Commun.* **2006**, 1488. (f) Fang, R. Q.; Zhang, X. M. *Inorg. Chem.* **2006**, *45*, 4801.
(13) *SAINT*, 6.02 ed.; Bruker AXS: Madison, WI, 1999.
(14) Sheldrick, G. M. *SADABS, Empirical Absorption Correction Program*; University of Göttingen: Göttingen, Germany, 1997.
(15) Altomare, A.; Cascarano, G.; Giacovazzo, C.; Gualaradi, A. *J. Appl. Crystallogr.* **1993**, *26*, 343.
(16) Spek, A. L. *J. Appl. Crystallogr.* **2003**, *36*, 7.
(17) Sheldrick, G. M. *SHELXL 97, Program for the Solution of Crystal Structure*; University of Göttingen: Göttingen, Germany, 1997.
(18) Sheldrick, G. M. *SHELXS 97, Program for the Solution of Crystal Structure*; University of Göttingen: Göttingen, Germany, 1997.
(19) *WinGX, A Windows Program for Crystal Structure Analysis*: Farrugia, L. J. *J. Appl. Crystallogr.* **1999**, *32*, 837.
(20) Hutter, J.; Ballone, J. P.; Bernasconi, M.; Focher, P.; Fois, E.; Goedecker, S.; Marx, D.; Parrinello, M.; Tuckerman, M. E. *CPMD*, Version 3.13.2; Max Planck Institut fuer Festkoerperforschung: Stuttgart, Germany, 1990.
(21) Troullier, N.; Martins, J. L. *Phys. Rev. B* **1991**, *43*, 1993.
(22) (a) Becke, A. D. *Phys. Rev. A* **1988**, *38*, 3098. (b) Lee, C.; Yang, W.; Parr, R. G. *Phys. Rev. B* **1988**, *37*, 785.
(23) Car, R.; Parrinello, M. *Phys. Rev. Lett.* **1985**, *55*, 2471.
(24) Martyna, G. J.; Klein, M. L.; Tuckerman, M. E. *J. Chem. Phys.* **1992**, *97*, 2635.
(25) Sillar, K.; Hofmann, A.; Sauer, J. *J. Am. Chem. Soc.* **2009**, *131*, 4143.
(26) Grimme, S. *J. Comput. Chem.* **2006**, *27*, 1787.
(27) (a) *Jmol, An open-source Java viewer for chemical structures in 3D*; http://www.jmol.org/. (b) McMahon, B.; Hanson, R. M. *J. Appl. Crystallogr.* **2008**, *41*, 811.
(28) Humphrey, W.; Dalke, A.; Schulten, K. *J. Mol. Graphics* **1996**, *14*, 33.
(29) (a) Blatov, V. A.; Carlucci, L.; Ciani, G.; Proserpio, D. M. *CrystEngComm* **2004**, *6*, 377. (b) Blatov, V. A.; Shevchenko, A. P.; Serezhkin, V. N. *J. Appl. Crystallogr.* **2000**, *33*, 1193.
(30) (a) Beck, D. W. *Zeolite Molecular Sieves*; Wiley & Sons: New York, 1974. (b) Webster, C. E.; Drago, R. S.; Zerner, M. C. *J. Am. Chem. Soc.* **1998**, *120*, 5509.
(31) (a) Saito, A.; Foley, H. C. *AIChE. J.* **1991**, *37*, 429. (b) Park, H. J.; Cheon, Y. E.; Suh, M. P. *Chem.—Eur. J.* **2010**, *16*, 11662.
(32) (a) Kaye, S. S.; Long, J. R. *J. Am. Chem. Soc.* **2005**, *127*, 6506. (b) Cheon, Y. E.; Suh, M. P. *Chem. Commun.* **2009**, 2296.
(33) (a) Ferey, G.; Serre, C. *Chem. Soc. Rev.* **2009**, *38*, 1380. (b) Coudert, F. X.; Draznieks, C. M.; Fuchs, A. H.; Boutin., A. *J. Am. Chem. Soc.* **2009**, *131*, 11329. (c) Park, H. J.; Suh, M. P. *Chem. Commun.* **2010**, *46*, 610. (d) Bourrelly, S.; Llewellyn, P. L.; Serre, C.; Millange, F.; Loiseau, T.; Feréy, G. *J. Am. Chem. Soc.* **2005**, *127*, 13519.
(34) Dubinin, M. M. *Chem. Rev.* **1960**, *60*, 235.
(35) (a) Kuc, A.; Heine, T.; Seifert, G.; Duarte, H. A. *Theor. Chem. Acc.* **2008**, *120*, 543. (b) Kuc, A.; Heine, T.; Seifert, G.; Duarte, H. A. *Chem.—Eur. J.* **2008**, *14*, 6597. (c) Perez, R. B.; Pérez, E. G.; Sevillano, J. G.; Merkling, P. J.; Calero, S. *Adsorption Sci. Technol.* **2010**, *28*, 823. (d) Salles, F.; Jobic, H.; Ghoufi, A.; Llewellyn, P. L.; Serre, C.; Bourrelly, S.; Feréy, G.; Maurin, G. *Angew.Chem., Int. Ed.* **2009**, *48*, 8335. (e) Areán, C. O.; Chavan, S.; Cabello, C. P.; Garrone, E.; Palomino, G. T. *ChemPhysChem* **2010**, *11*, 3237.
(36) Bhargava, B. L.; Balasubramanian, S. *Chem. Phys. Lett.* **2007**, *444*, 242.
(37) Bučko, M.; Hafner, J.; Lebègue, S.; Ángyán, J. G. *J. Phys. Chem. A* **2010**, *114*, 11814.
(38) (a) Talu, O. *Adv. Colloid Interface Sci.* **1998**, *76−77*, 227. (b) Purewal, J. Hydrogen adsorption by alkali metal graphite intercalation compounds. Ph.D. Dissertation, California Institute of Technology, Pasadena, CA, 2010.